


Research Article

Ultracompact Ball Vibrating Triboelectric Nanogenerator for Maximizing Instantaneous Power Output in Minimized Size

Seh-Hoon Chung,¹ Minju Jee,¹ Sujung Kang,¹ Zong-Hong Lin ,² Youngho Jin ,³ and Sangmin Lee ¹

¹School of Mechanical Engineering, Chung-Ang University, 84, Heukseok-ro, Dongjak-gu, Seoul 06974, Republic of Korea

²Department of Biomedical Engineering, National Taiwan University, Taipei 10167, Taiwan

³Department of Advanced Materials Engineering, Chung-Ang University, Anseong 17546, Gyeonggi-do, Republic of Korea

Correspondence should be addressed to Zong-Hong Lin; zhlin@ntu.edu.tw, Youngho Jin; yhj@cau.ac.kr, and Sangmin Lee; slee98@cau.ac.kr

Received 10 December 2024; Revised 27 March 2025; Accepted 17 July 2025

Academic Editor: Puran Pandey

Copyright © 2025 Seh-Hoon Chung et al. International Journal of Energy Research published by John Wiley & Sons Ltd. This is an open access article under the terms of the Creative Commons Attribution License, which permits use, distribution and reproduction in any medium, provided the original work is properly cited.

The increased adoption of Internet of Things (IOT)-based portable devices has called attention to the need for high-output portable power supply. Portable electronics powered by batteries require additional processes, such as replacement or recharging, for continuous operation. Small-sized triboelectric nanogenerators (TENGs), which have been investigated for real-time power supply, are limited by low output owing to their small surface area and small surface charge. Therefore, a TENG device that can generate a high output for a real-time power supply is necessary. Herein, an ultracompact ball-vibrating TENG (UBV-TENG) is reported. With output enhancement owing to the electron avalanche effect, the UBV-TENG can generate an instantaneous peak power of up to 0.7126 W with a diameter of 5 mm and height of 20 mm. With comparing existing TENGs, the UBV-TENG generated more than 3 times higher instantaneous peak power with smaller device size. Owing to its small size and high performance, the optimized UBV-TENG can be easily utilized for portable human-motion energy-harvesting device, such as a self-powered safety light, as demonstrated by fabricating a 2 cm × 2 cm self-powered light emitting diode (LED) circuit that powers up to 120 LEDs with stacked structures.

Keywords: electron avalanche; high instantaneous power; miniaturized; self-powered safety light; triboelectric nanogenerator

1. Introduction

With the rapid growth of Internet of Things (IOT), various types of IOT-enabled miniaturized devices have been investigated. A major challenge to wider adoption of portable IOT devices is the design that allows integration of only small energy sources, such as small batteries, including dry cells and rechargeable batteries. Nevertheless, battery-based devices require additional processes, such as replacement or recharging, for continuous operation owing to the limited lifetime of batteries. Therefore, many researchers have focused on human-motion energy-harvesting devices for real-time power supply in small devices. In particular, triboelectric nanogenerators (TENGs), which generate electricity via the triboelectric

effect and electrostatic induction [1], are in the spotlight as portable energy-harvesting devices [2] and human body motion energy harvester, such as arm [3] and elbow movement [4], and which can harvest vibration-based input energy for energy harvesting [5] and vibration sensor [6] that offer the advantages of low cost using recycled materials [7], simple design [8], and new materials [9], easy fabrication [10], and high applicability, such as hybrid energy generating [11], blue energy harvesting [12], contact force sensing [13], and gas mask [14]. However, existing small-sized TENGs have critical limitations in that they can only generate an insufficiently low-power output due to the nano- to microampere scale of low current output. As reported in previous studies, the triboelectric nanogenerator (TENG) output is dependent on the surface

charge of the triboelectric materials, which can be determined by the surface charge density [15] and area of the triboelectric layer [16]. Thus, as there is a trade-off between high output power and small device size, fabricating small-sized high-power output TENG is challenging with fundamental energy generating mechanism of existing TENGs. Therefore, a novel type of small-sized TENG device that can generate a high output even with a small size should be developed for use as a real-time power supply in existing portable electronic devices.

In this study, an ultracompact ball-vibrating TENG (UBV-TENG) with a small structure was fabricated, which can generate a high-power output from a vibration input. When the ball vibrates because of the movement of the UBV-TENG, a high electric field is generated between the electrodes and balls, inducing an electrostatic discharge. Owing to the electron avalanche effect of the electrostatic discharge, the UBV-TENG can generate both high-voltage and high-current outputs even with a small structure. As a result, the UBV-TENG with 5 mm of diameter and 20 mm of height generated an optimum instantaneous peak power of 0.7126 W, which is more than three times higher than that reported in previous research even with smaller device size. Owing to its small size and high output, the UBV-TENG can be utilized in the suggested application scenario of a self-powered safety light. In this study, a 2 cm × 2 cm self-powered light-emitting device is demonstrated, which can be easily applied in small accessories. Moreover, three stacked UBV-TENGs were successfully powered up to 120 light emitting diodes (LEDs) with only a 1.5 cm × 2 cm device.

2. Results

A small-sized UBV-TENG was fabricated with a simple design, as shown in Figure 1a,b. The UBV-TENG consisted of three parts (Figure 1a): a polyvinyl chloride (PVC) cylinder, top and bottom electrodes, and steel balls. When the steel balls inside the device vibrate owing to movement, they slide through the PVC cylinder. Thus, as the steel balls come in contact with the PVC cylinder, the surface charges on the PVC cylinder induce charges inside the steel ball, as shown in Figure 1c. According to the triboelectric series, PVC has a relatively high electron affinity, and steel has a relatively low electron affinity; thus, negative charges are located on the PVC surface, and positive charges are induced inside the steel ball near the PVC surface. However, as the steel ball is opened, negative charges remain inside the steel ball. Consequently, as shown in Figure 1c, the negative charges are polarized from the induced negative charges inside the steel ball. When the steel balls moved near the top or bottom electrode, the polarized negative charges created a strong electric field between the steel ball and the top or bottom electrode. With this strong electric field, a polarized negative charge is emitted from the ball and accelerates to the electrode. This accelerated negative charge collides with air to the ions and causes an electron avalanche effect. Eventually, more negative charges can be transferred to the electrode, generating a high current.

With the avalanche effect, even the UBV-TENG with a small size can generate high voltage and current outputs.

Figure 1b shows a photograph of the UBV-TENG and a quarter-dollar coin. Even with the 20 mm height and 5 mm diameter of UBV-TENG, the device generated peak voltage and current of up to 80 V and 0.15 A, respectively, which is shown in Figure 1d. Figure 1e shows the instantaneous peak power of the UBV-TENG connected to the load resistance. The instantaneous peak power of the UBV-TENG was calculated by multiplying the average instantaneous peak voltage and instantaneous peak current outputs with different load resistances, as shown in Supporting Information 1: Figure S1. The optimum instantaneous peak power of UBV-TENG was calculated as 0.71264 W with 300 Ω. Figure 1f shows a comparison of the instantaneous peak power and device volume of the UBV-TENG and other TENGs from previous studies. The device volume and the peak power from previous references were $4.5 \times 10^{-6} \text{ m}^3$ and 0.58 mW [17], $1.57 \times 10^{-3} \text{ m}^3$ and 10.97 mW [18], $3.534 \times 10^{-5} \text{ m}^3$ and 19.98 mW [19], $2.47 \times 10^{-4} \text{ m}^3$ and 0.247 mW [20], $4.32 \times 10^{-5} \text{ m}^3$ and 198 mW [21], $3.93 \times 10^{-3} \text{ m}^3$ and 5.38 mW [22], $2.77 \times 10^{-3} \text{ m}^3$ and 4.56 mW [23], $9.94 \times 10^{-4} \text{ m}^3$ and 8.8 mW [24], $1 \times 10^{-7} \text{ m}^3$ and 0.5865 mW [25], respectively. The results show that the UBV-TENG can generate a significantly high peak power, even with an ultracompact size, compared with previous studies.

Figure 2a,b presents the detailed working mechanism of UBV-TENG. When the UBV-TENG is moved by the vibration input as Figure 2ai, the steel balls move inside the device. As shown in Figure 2aii, when the balls slide on the PVC cylinder, positive charges are induced by the PVC cylinder, and the polarized negative charges generate a high electrical potential between the top electrode and the steel balls, which can be explained by the simulation results shown in Figure 2b. This result was simulated using the finite element method (FEM) program COMSOL Multiphysics. The geometry of the model was the same as that of UBV-TENG and the surface charge density of PVC cylinder was set as $-5.2 \mu\text{C}/\text{m}^2$ [26]. As shown in Figure 2bi, over 3 kV/mm of high electric field is generated between the balls and the top electrode. According to Paschen's law, the breakdown voltage (V_b) in air can be determined as follows:

$$V_b = \frac{Bpd}{\ln(Apd) - \ln\left[\ln\left(1 + \frac{1}{\gamma_{se}}\right)\right]},$$

where A and B are constants that depend on air, p is the air pressure, d is the gap between the electrodes, and γ_{se} is the secondary electron emission coefficient. Considering this formula, the air breakdown effect can be determined by the electric field between the two electrodes. It is known that an electric field strength of $\sim 3 \text{ kV}/\text{mm}$ can cause electrostatic discharge in dry air. Therefore, according to the simulation results in Figure 2b, an electrostatic discharge can be generated with the movement of the steel balls; thus, the UBV-TENG can generate a high electrical output with this electrostatic discharge. For better comparison, Supporting Information 1: Figure S2 shows voltage output of the UBV-TENG with covering dielectric layer on the top and bottom electrodes and the UBV-TENG without

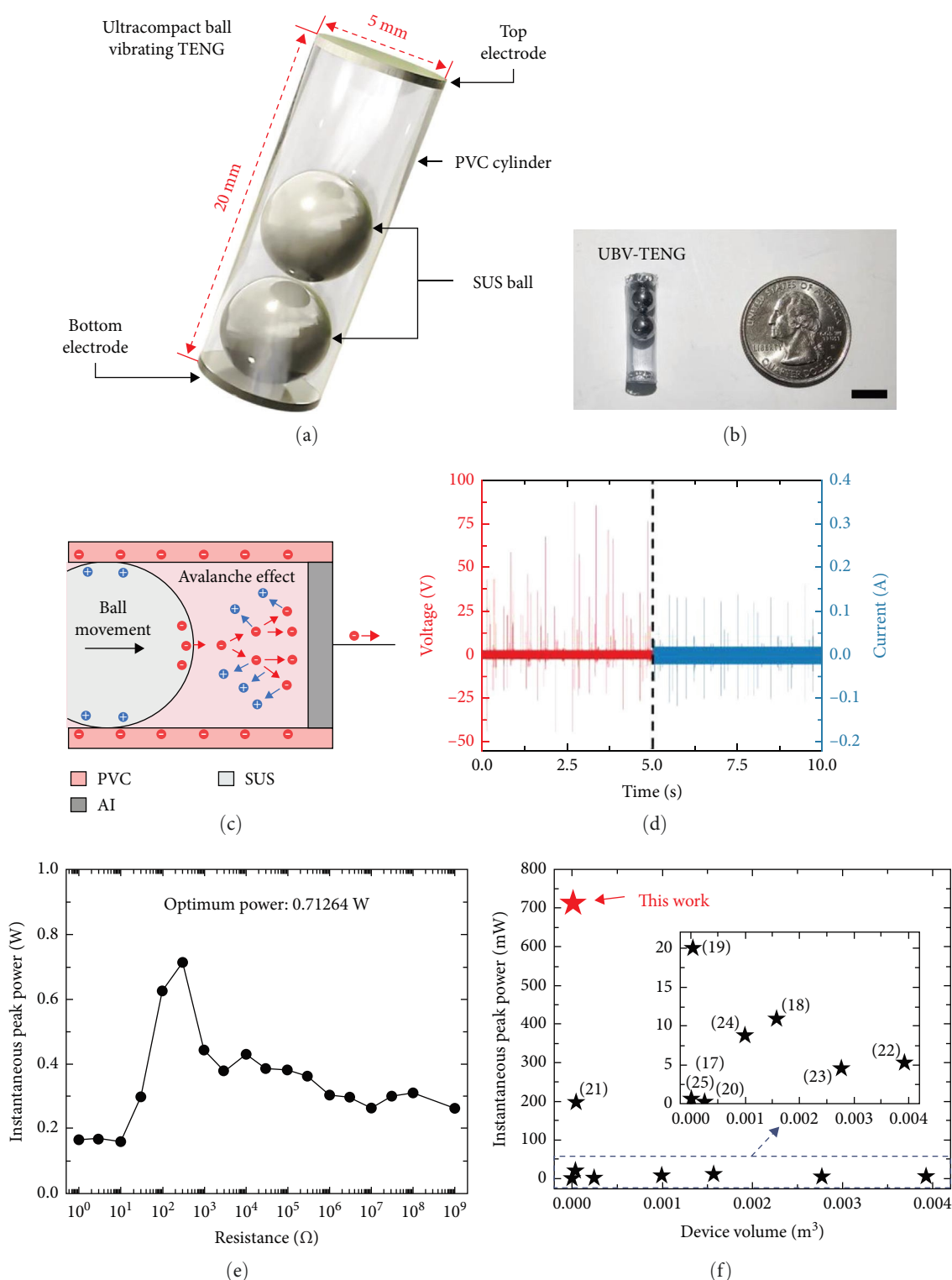


FIGURE 1: Concept of UBV-TENG. (a) Schematic illustration of UBV-TENG. (b) Photograph of UBV-TENG (scale bar: 1 cm). (c) Schematic of brief working mechanism of UBV-TENG. (d) Measured voltage and current outputs of UBV-TENG. (e) Calculated instantaneous peak power of UBV-TENG with different load resistance. (f) Compared instantaneous peak power and device volume with previous references.

the dielectric layer. The polytetrafluoroethylene (PTFE) film is used for dielectric layer. Without dielectric layer the UBV-TENG generated about 50 V of peak voltage whereas the UBV-TENG with dielectric layers generated about 3 V of peak

voltage. This result indicates that the electrostatic discharge-based output can generate high peak voltage output.

Figure 2c shows the expanded voltage and current graphs of a single-peak output. A high peak voltage and current with a

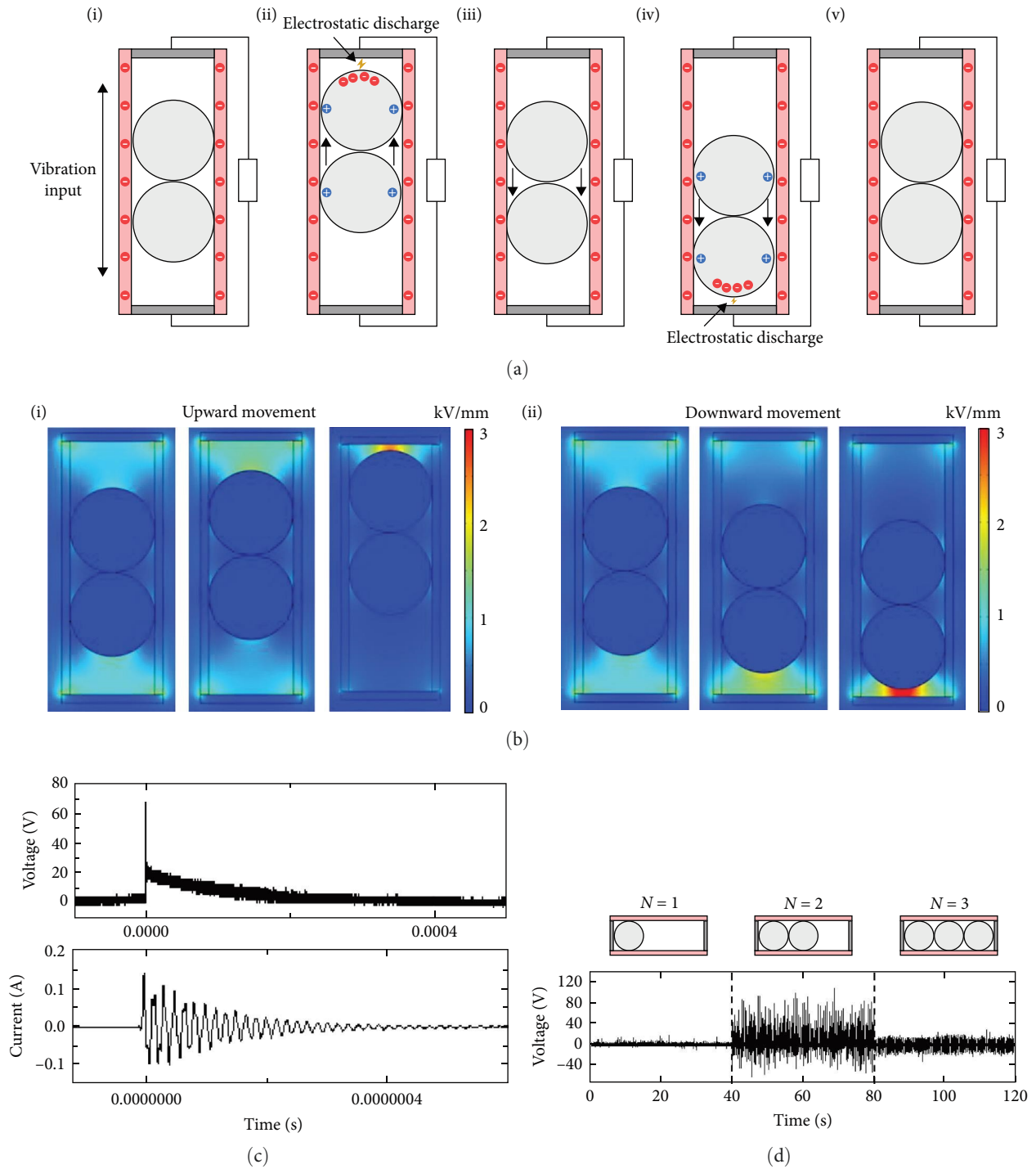


FIGURE 2: Detailed working mechanism of UBV-TENG. (a) Schematic of working mechanism of UBV-TENG. (b) Simulation result of UBV-TENG which shows electric field strength. (c) Extended voltage and current graph of one peak output. (d) Voltage graph of UBV-TENG with different number of steel balls.

short duration were measured up to 68 V and 0.14 A, respectively. In addition, the underdamping waveform of the output current was measured. According to previous studies, a short-duration high-peak output can be generated by an electrostatic discharge [27]. Moreover, the current based on electrostatic discharge can be measured as an underdamping waveform due to the measurement circuit inductance and capacitance [28].

Accordingly, the results indicate that electrostatic discharge occurred inside the UBV-TENG, even in a small device.

To consider the effect of the number of balls inside the UBV-TENG, the output voltage and current were measured for different ball numbers, as shown in Figure 2d and Supporting Information 1: Figure S3, respectively. With the same height and diameter as the PVC cylinder, the UBV-TENG

generated the highest voltage and current with two steel balls. When only one ball was used, the steel ball was unable to generate a sufficient electric field with the vibration input. When three balls were used in the UBV-TENG, there was little space between the balls and the top and bottom electrodes; thus, it was difficult to generate a surface charge on the PVC cylinder by ball movement and generate an electric field. As a result, the highest peak voltage and current outputs of the UBV-TENG were measured up to 90 V and 0.2 A with two steel balls, respectively.

As discussed in the previous paragraph, the spacer height between the balls and electrodes and the number of balls are the major parameters that affect the output of the UBV-TENG. Considering this result, the ratio between the diameter and height of the UBV-TENG is an important factor for the structural optimization of the UBV-TENG because different numbers of balls and spacer heights can be utilized in the UBV-TENG with each ratio. For a better comparison, three other cases (Figure 3a) of the UBV-TENG voltage and current outputs are shown in Figure 3b,c and Supporting Information 1: Figures S4 and S5. Each result was measured with a shaking input using an electrical motor at a frequency of 2 Hz. The first case of the UBV-TENG occurred when the diameter-to-height ratio was 1 : 2 (Figure 3b and Supporting Information 1: Figure S4). The peak voltage and current outputs of the UBV-TENG in Case 1 were measured up to 18.0 V and 0.024 A, respectively, with one ball. In addition, the peak voltage and current outputs of the Case 1 UBV-TENG with two balls were measured up to 22.0 V and 0.024 A, respectively. Both the devices based on Case 1 generated a relatively low voltage and current output owing to their low surface charge and spacer height. Therefore, Case 1 had an improper ratio for the UBV-TENG.

Case 2 with a UBV-TENG ratio of 1:3, which is discussed in the previous paragraph, is illustrated in the output graph in Figure 2d. Case 3, in which the UBV-TENG ratio was 1:4; is illustrated in the output graphs in Figure 3c and Supporting Information 1: Figure S5. When one ball was used in Case 3 of UBV-TENG, the peak voltage and current outputs are generated up to 19.0 V and 0.024 A, respectively. However, when two and three balls are used in Case 3 of UBV-TENG, the peak voltage outputs are increased up to 42.0 and 50.0 V, respectively, and the peak current outputs are increased up to 0.096 and 0.12 A, respectively. However, both the peak voltage and current outputs decrease when four balls are used owing to the short spacer height. The peak voltage and current outputs of Case 3 of the UBV-TENG with four steel balls were measured up to 9.00 V and 0.056 A, respectively. For an accurate comparison of each ratio of the UBV-TENG with different numbers of steel balls, the average peak voltages of the UBV-TENG for different cases and ball numbers are shown in Figure 3d. The average peak voltages of Case 1 with 1 and 2 balls were 8.90, 7.85 V, respectively, the voltages of Case 2 with 1, 2, and 3 balls were 8.94, 41.8, 14.0 V, respectively, and the voltages of Case 3 with 1, 2, 3, 4 balls were 9.83, 14.0, 16.9, and 6.72 V, respectively. As can be seen, the highest average peak voltage was generated with the Case 2 structure with two balls in the device; thus, the structure of the UBV-TENG was optimized with the ratio of Case 2 and two balls.

In addition, because the UBV-TENG generates electricity through the triboelectric effect of the cylinder, proper selection of the cylinder material is necessary to optimize the UBV-TENG structure. The voltage and current outputs of the UBV-TENG with different materials are shown in Figure 3e and Supporting Information 1: Figure S6. The high voltage and current outputs were generated in the following order: PVC, PTFE, PI, and nylon. According to previous research, the highest surface charge densities of several materials were reported in the order PVC > PTFE > PI > nylon [29]. Therefore, PVC was selected for the UBV-TENG. Moreover, as the material of metal ball can influence the electrical output of the UBV-TENG, Supporting Information 1: Figure S7 shows voltage outputs of UBV-TENG with different metal balls. As a result, the UBV-TENG with SUS balls generated higher peak voltage output than the UBV-TENG with Al balls. Since TENGs generate higher electrical output with increased force [30], the UBV-TENG with SUS balls generated higher voltage output due to the higher weight of SUS balls. Therefore, SUS balls was selected for the UBV-TENG.

Using the optimized ratio, ball number, and material for the UBV-TENG, the outputs of different sizes of the UBV-TENG are shown in Figure 3f–h to minimize the size of the UBV-TENG. As shown in Figure 3f, UBV-TENGs with diameters of 3, 5, and 7 mm were fabricated, and the voltage and current outputs of each device were measured, as shown in Figure 3g and Supporting Information 1: Figure S8. The average peak voltages of the devices are shown in Figure 3h for a better comparison. The UBV-TENGs with diameters of 3, 5, and 7 mm generated peak voltages of 1.39, 50.0, 54.7 V, respectively. The UBV-TENGs with diameters of 5 and 7 mm generated a high electrical output similar to the previous results; however, the peak voltage of the UBV-TENG with a diameter of 3 mm could not be measured. Nevertheless, when operating the devices with a manual input, it was possible to measure the peak voltage of the UBV-TENG with a diameter of 3 mm, as shown in Supporting Information 1: Figure S9. A peak voltage of ~3 V was generated by the UBV-TENG with a diameter of 3 mm. Considering its small size compared to other devices, its output is significantly lower than that of the other devices. It is assumed that the ball movement was unable to generate a sufficiently high electric field strength for electrostatic discharge owing to its structure. In addition, it was difficult to fabricate the precise structure of the UBV-TENG with a diameter of 3 mm using the same fabrication method. Thus, to further reduce the size of UBV-TENGs, studies on the fabrication methods and working mechanisms of diameters below 3 mm are necessary. Therefore, the diameter of the minimized UBV-TENG was optimized as 5 mm.

Moreover, the voltage outputs of the UBV-TENG with different input frequencies are shown in Supporting Information 1: Figure S10 to show that UBV-TENG can be effectively utilized as human body motion energy harvester. Since 1.4 Hz to 2.2 Hz of vibration frequency is made by human walking [31], Supporting Information 1: Figure S10 shows the voltage outputs of the UBV-TENG when 1.4, 1.6, 1.8, 2, and 2.2 Hz of input frequencies are given. As the UBV-TENG generated the same peak outputs with different frequencies, this result

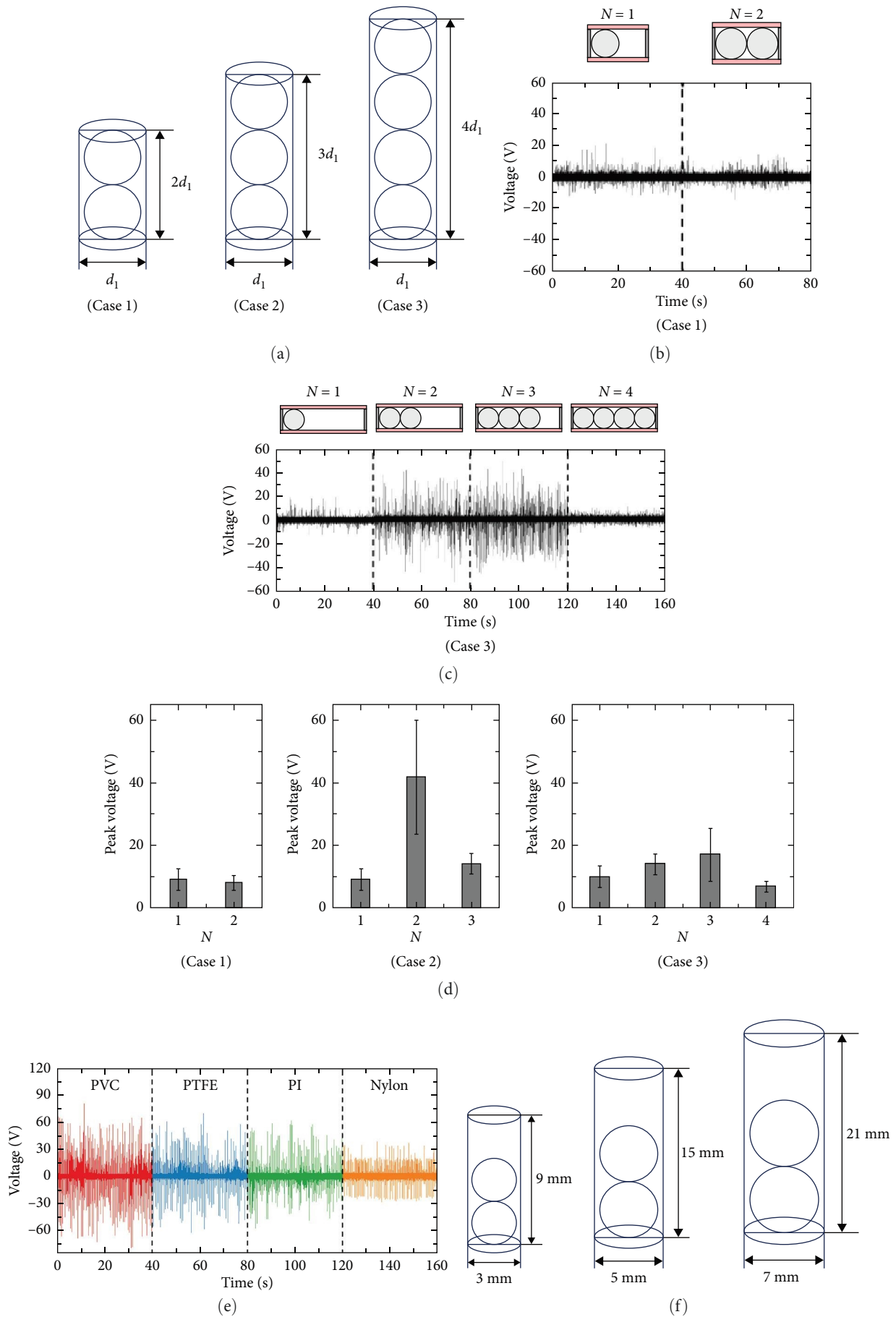


FIGURE 3: Continued.

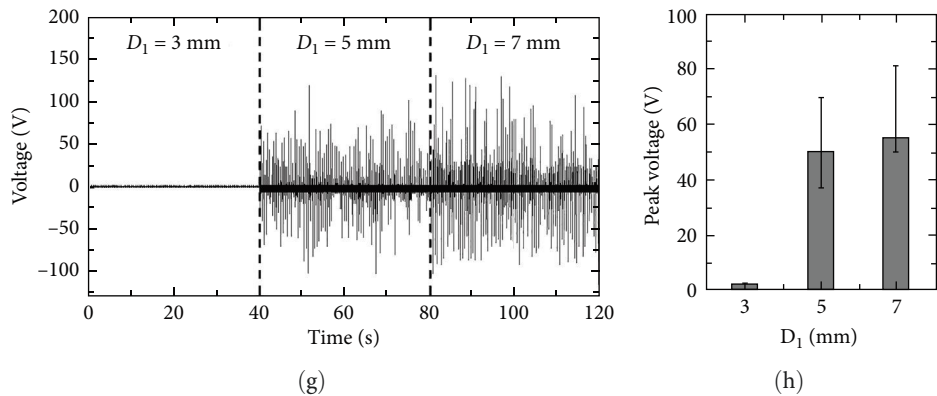


FIGURE 3: Parametric optimization of UBV-TENG. (a) Schematic of three cases of UBV-TENG with different ratios. (b) Voltage graphs of Case 1 UBV-TENG with different numbers of steel balls. (c) Voltage graphs of Case 3 UBV-TENG with different numbers of steel balls. (d) Average of the peak voltages of Case 1, 2, and 3 UBV-TENG. (e) Voltage graph of UBV-TENG with different materials. (f) Schematic of different sizes of UBV-TENG. (g) Voltage graph of different sizes of UBV-TENG. (h) Average of the peak voltages of different sizes of UBV-TENG.

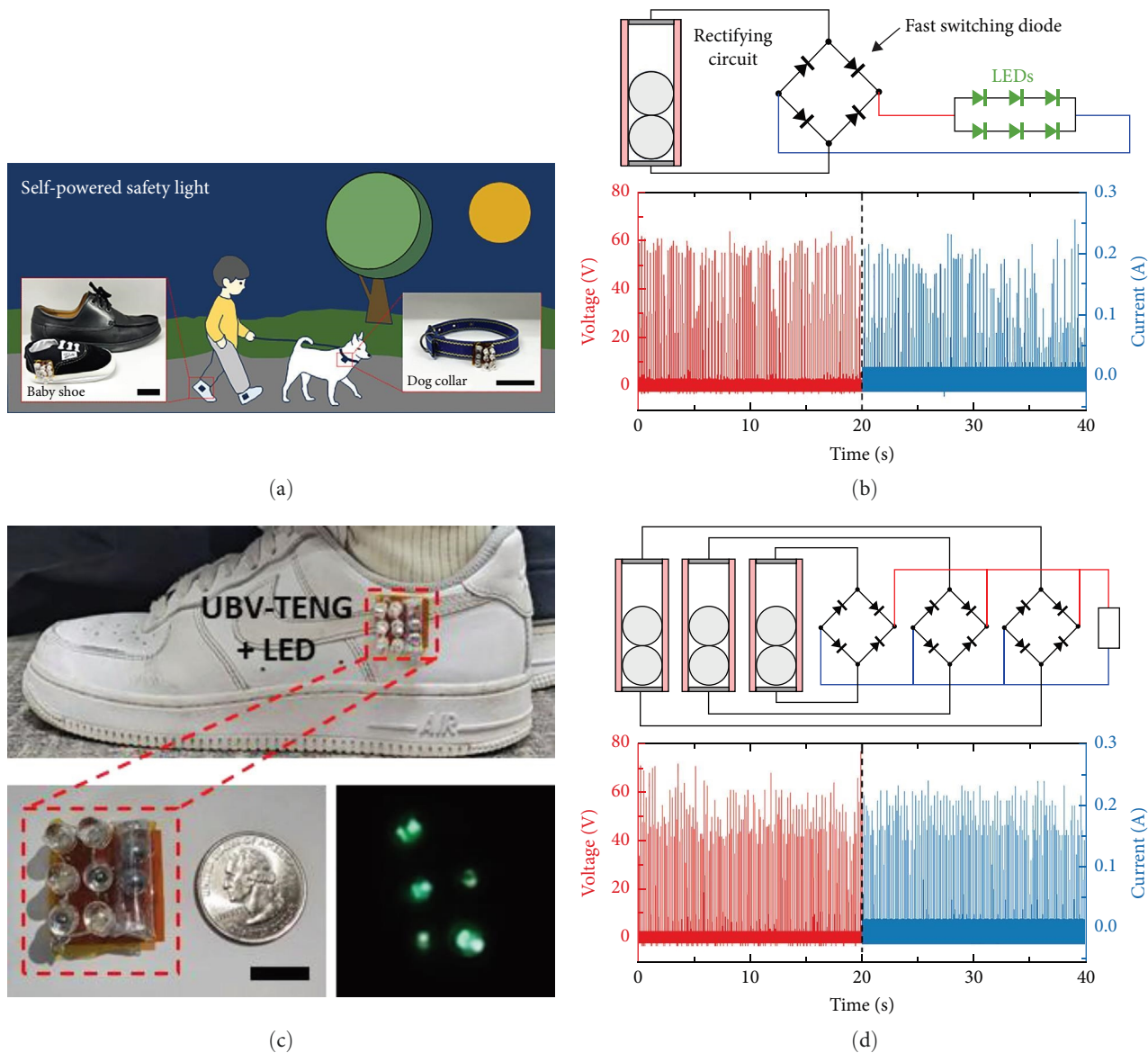


FIGURE 4: Continued.

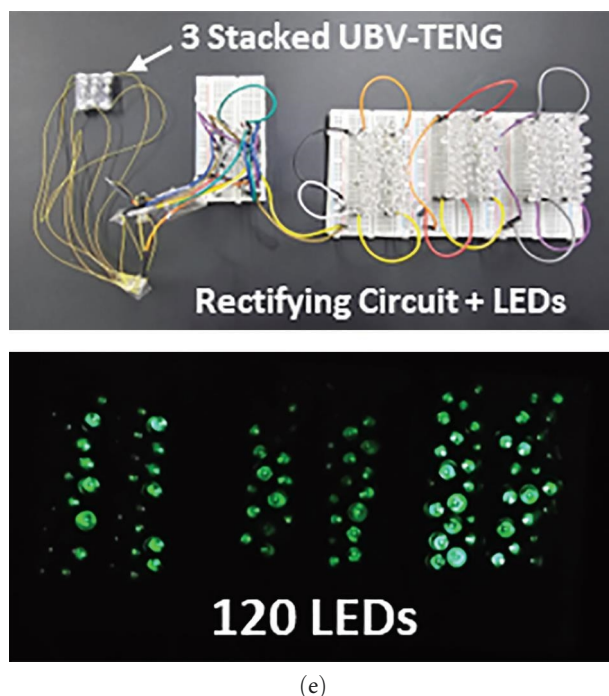


FIGURE 4: Applications for UBV-TENG. (a) Schematic of application scenario of UBV-TENG as self-powered safety light (scale bar: 3 cm). (b) Rectifying circuit for UBV-TENG and rectified voltage and current graph of UBV-TENG. (c) Fabricated 2 cm \times 2 cm size light emitting device, including UBV-TENG, rectifying circuit, and LEDs. (d) Rectifying circuit for three stacked UBV-TENG and the rectified voltage and current graph of three stacked UBV-TENG. (e) Photographs of experimental setup of three stacked UBV-TENG, rectifying circuit, and 120 LEDs, and powered 120 LEDs with three stacked UBV-TENG movement.

indicates that the UBV-TENG can effectively generate electrical output with human walking motion.

In addition, to show the durability of UBV-TENG, Supporting Information 1: Figure S11 shows voltage output of UBV-TENG with 24 h operation. As 2 Hz of input frequency was given, the UBV-TENG generated the same voltage output until about 172,800 cycles. This result shows that the UBV-TENG can be operated without damage until a long duration time.

Because, the optimized minimum size of the UBV-TENG is compact with a high performance, it can be applied in various fields. Figure 4a shows an application scenario for the UBV-TENG, which is a self-powered safety light. Owing to its small size and light weight, it can be easily utilized in small accessories, such as baby shoes and dog collars. In particular, because careful attention is necessary for night walks with babies and dogs, the UBV-TENG can be the most suitable device in real life.

To turn on the LEDs with UBV-TENG, the rectifying circuit and rectified voltage and current graph of UBV-TENG are shown in Figure 4b. Because the UBV-TENG generated a short-duration peak output, fast-switching diodes were used for the rectifying circuit. With the UBV-TENG and rectifying circuit, a voltage of ~ 60 V and 0.2 A of current were generated and rectified. With the small size of the device, a small self-powered light-emitting device (3 cm \times 3 cm) was fabricated, as shown in Figure 4c. In addition, to allow the device to operate with foot movements while walking, the device was attached to a shoe. Supporting Information 2: Movie 1 shows the operation

of the LED device lights LEDs with foot movements. Moreover, the UBV-TENG could be easily stacked into a small size. Figure 4d shows the rectifying circuit for three stacked UBV-TENG and the rectified voltage and current outputs. Also, with the three stacked structure of UBV-TENG, it was able to power up to 120 LEDs as shown in Figure 4e and Supporting Information 3: Movie 2, Forty LEDs were connected to each UBV-TENG and rectifying circuit. These results show that the UBV-TENG can be utilized in real-life applications as a self-powered safety light.

3. Conclusion

In this study, we designed a small UBV-TENG to generate high output. While general small-sized TENGs are unable to generate a high output owing to an insufficient surface charge, the UBV-TENG can generate a high peak output owing to the avalanche effect of its own working mechanism. To maximize the output to a small size, the UBV-TENG was optimized by considering the structural ratio, ball number, and diameter. Although further studies are needed to create a smaller UBV-TENG, the UBV-TENG showed the highest performance with the smallest size compared to existing TENGs. The UBV-TENG achieved an instantaneous peak power of 0.71264 W with a small diameter of 5 and 20 mm of height. To demonstrate the application of the self-powered as night-walk safety light, a 2 cm \times 2 cm self-powered LED circuit was constructed with a UBV-TENG and a rectifying circuit, and was operated with foot movement. Moreover, three stacked UBV-TENGs

with a size of 1.5 cm × 2 cm were used to successfully power up to 120 LEDs. Therefore, the new type of small-sized high-power energy-harvesting device proposed in this paper can be utilized as a real-time power supply in real life. Furthermore, as a new type of small size energy harvester is still necessary in application fields, such as implantable biomedical energy generator, micro robotics, and MEMS devices, the UBV-TENG can be a starting point for a new field.

4. Methods

4.1. Fabrication of UBV-TENG. The UBV-TENG consists of a PVC cylinder, top and bottom electrodes, and steel balls. The PVC cylinder was fabricated by rolling a 15 mm (width) × 15 mm (height) PVC film (Sewon Film Co., South Korea) with a thickness of 0.1 mm. The top and bottom electrodes were made by attaching commercial aluminum tape (thickness: 0.05 mm, DUKSUNG Hitech Co., South Korea) to a polymethyl methacrylate (PMMA) substrate with a diameter of 5 mm, made using a laser cutter machine (X252, GCC Co., Taiwan). A commercial PVC wrapping wire (AWG30) was attached to the top and bottom electrodes using adhesive tape. PTFE (Chukoh Chemical Industries Co., Japan), PI (COVALUE YOUNGJIN Co., South Korea), and nylon (Goodfellow Co., United Kingdom) films were used to optimize the UBV-TENG parameters.

4.2. Finite Element Simulation. The simulation result of the UBV-TENG is calculated by using finite element simulation program called COMSOL Multiphysics (COMSOL Co.). The geometry of the UBV-TENG has been set as same as fabrication method of the UBV-TENG that the width and height of the UBV-TENG is set as 5 and 20 mm, respectively. The surface charge density and relative permittivity of the PVC film is set as -5.2 and 5 C/m^2 [26], respectively, according to [32]. The relative permittivity of air, metal balls, and top and bottom electrodes inside the UBV-TENG are all set as 1. Moreover, every boundary of metal balls are set with floating potential, and the top and bottom electrodes are grounded.

4.3. Characterization and Measurement. To measure the electrical performance of the UBV-TENG, a mechanical input was applied using a DC motor (BXSD120-C, Oriental Motor Co., Japan) operating at 120 rpm for a vibration frequency of 2 Hz.

The voltage and current were measured using a mixed-domain oscilloscope (MDO 34, Tektronix Co., United States) with a high-voltage differential probe (THDP0100, Tektronix Co., United States) and a current probe (TCP0030A, Tektronix Co. United States).

Data Availability Statement

The data that support the findings of this study are available in the Supporting Information of this article.

Conflicts of Interest

The authors declare no conflicts of interest.

Author Contributions

Seh-Hoon Chung and Minju Jee: conceptualization, methodology, validation, formal analysis, investigation, writing – original draft, writing – review and editing, visualization. **Sujung Kang:** formal analysis, methodology. **Zong-Hong Lin, Youngho Jin, and Sangmin Lee:** conceptualization, methodology, writing – review and editing, supervision, project administration. Seh-Hoon Chung and Minju Jee contributed equally to this work.

Funding

This research was financially supported by Chung-Ang University Research Grant in 2023, and supported by the National Research Foundation of Korea (NRF) grant funded by the Korea Government (MSIT) (RS-2025-02214162), and was supported by the Advancing the Technologies for Scientific Crime Investigation program through the Korea Institutes of Police Technology (KIPoT) funded by the Korean National Police Agency (RS-2024-00468545).

Acknowledgments

We would like to thank Editage (www.editage.co.kr) for English language editing.

Supporting Information

Additional supporting information can be found online in the Supporting Information section.

Supporting Information 1. Supporting Information Figure S1: Instantaneous peak voltage and current output of UBV-TENG with different load resistances. Supporting Information Figure S2: Measured voltage output of the UBV-TENG (a) without and (b) with dielectric layer on the top and bottom electrodes. Supporting Information Figure S3: Current graphs of UBV-TENG with different number of steel balls of Case 2. Supporting Information Figure S4: Current graphs of UBV-TENG with different number of steel balls of Case 1. Supporting Information Figure S5: Current graphs of UBV-TENG according to the number of steel balls in the size of Case 3. Supporting Information Figure S6: Current graph of UBV-TENG with different triboelectric materials. Supporting Information Figure S7: Voltage output of UBV-TENG with SUS balls and with Al balls. Supporting Information Figure S8: Current graph of UBV-TENG with different D11, D22, and D33. Supporting Information Figure S9: Voltage and current graphs of UBV-TENG with different d11, d22, and d33 with a manual input. Supporting Information Figure S10: Voltage output of UBV-TENG with different input frequencies. Supporting Information Figure S11: Voltage output of UBV-TENG with 24 h operation.

Supporting Information 2. Supporting Information Movie S1: Operation of light-emitting device containing UBV-TENG with foot movement.

Supporting Information 3. Supporting Information Movie S2: 120 LEDs powered by 3 stacked UBV-TENG.

References

- [1] Z. Lin, J. Chen, and J. Yang, "Recent Progress in Triboelectric Nanogenerators as a Renewable and Sustainable Power Source," *Journal of Nanomaterials* 2016, no. 1 (2016): 5651613, 24.
- [2] K. Xia, D. Wu, J. Fu, N. A. Hoque, Y. Ye, and Z. Xu, "A High-Output Triboelectric Nanogenerator Based on Nickel-Copper Bimetallic Hydroxide Nanowrinkles for Self-Powered Wearable Electronics," *Journal of Materials Chemistry A* 8, no. 48 (2020): 25995–26003.
- [3] K. Xia, Z. Zhu, H. Zhang, C. Du, J. Fu, and Z. Xu, "Milk-Based Triboelectric Nanogenerator on Paper for Harvesting Energy From Human Body Motion," *Nano Energy* 56 (2019): 400–410.
- [4] K. Xia, Z. Zhu, H. Zhang, C. Du, Z. Xu, and R. Wang, "Painting a High-Output Triboelectric Nanogenerator on Paper for Harvesting Energy From Human Body Motion," *Nano Energy* 50 (2018): 571–580.
- [5] S. Hu, Z. Yuan, R. Li, et al., "Vibration-Driven Triboelectric Nanogenerator for Vibration Attenuation and Condition Monitoring for Transmission Lines," *Nano Letters* 22, no. 13 (2022): 5584–5591.
- [6] Q. Xu, Y. Qi, X. Li, et al., "Ultrawide-Frequency Vibration Sensor Based on Magnetically Floating Triboelectric Nanogenerator," *ACS Applied Electronic Materials* 6, no. 2 (2024): 1104–1112.
- [7] J. H. Son, K. Cha, S. H. Chung, et al., "Contaminated, Crumpled Aluminum Foil-Driven Triboelectric Nanogenerator," *Advanced Science* 10, no. 28 (2023): 2301609.
- [8] D. Bhatia, J. Lee, H. J. Hwang, J. M. Baik, S. Kim, and D. Choi, "Design of Mechanical Frequency Regulator for Predictable Uniform Power From Triboelectric Nanogenerators," *Advanced Energy Materials* 8, no. 15 (2018): 1702667.
- [9] P. Supraja, R. R. Kumar, S. Mishra, et al., "A Simple and Low-Cost Triboelectric Nanogenerator Based on Two Dimensional ZnO Nanosheets and Its Application in Portable Electronics," *Sensors and Actuators A: Physical* 335 (2022): 113368.
- [10] W.-G. Kim, D.-W. Kim, I.-W. Tcho, J.-K. Kim, M.-S. Kim, and Y.-K. Choi, "Triboelectric Nanogenerator: Structure, Mechanism, and Applications," *ACS Nano* 15, no. 1 (2021): 258–287.
- [11] S.-H. Chung, M. Kim, Z.-H. Lin, et al., "Enhancing Strategy of Triboelectric Nanogenerator via Origami Pattern by Harvesting Mechanical Motion and Wind Flow," *International Journal of Energy Research* 2024, no. 1 (2024): 2120442.
- [12] U. Khan and S.-W. Kim, "Triboelectric Nanogenerators for Blue Energy Harvesting," *ACS Nano* 10, no. 7 (2016): 6429–6432.
- [13] D. Seo, J. Kong, and J. Chung, "Scott–Russel Linkage-Based Triboelectric Self-Powered Sensor for Contact Material-Independent Force Sensing and Tactile Recognition," *Small* 20, no. 43 (2024): 2403394.
- [14] D. Heo, M. Song, S. H. Chung, et al., "Inhalation-Driven Vertical Flutter Triboelectric Nanogenerator With Amplified Output as a Gas-Mask-Integrated Self-Powered Multifunctional System," *Advanced Energy Materials* 12, no. 31 (2022): 2201001.
- [15] H.-W. Park, N. D. Huynh, W. Kim, et al., "Electron Blocking Layer-Based Interfacial Design for Highly-Enhanced Triboelectric Nanogenerators," *Nano Energy* 50 (2018): 9–15.
- [16] H. Ryu, H. J. Yoon, and S. W. Kim, "Hybrid Energy Harvesters: Toward Sustainable Energy Harvesting," *Advanced Materials* 31, no. 34 (2019): 1802898.
- [17] Y. Wang, Y. Wu, Q. Liu, et al., "Origami Triboelectric Nanogenerator With Double-Helical Structure for Environmental Energy Harvesting," *Energy* 212 (2020): 118462.
- [18] S. Xu, W. Nie, J. Sun, et al., "Multi-Mode and Durable Fiber Triboelectric Nanogenerator for Power and Sensor Enabled by Hookean Vascular Stent Structure," *Chemical Engineering Journal* 472 (2023): 145088.
- [19] P. Rui, W. Zhang, and P. Wang, "Super-Durable and Highly Efficient Electrostatic Induced Nanogenerator Circulation Network Initially Charged by a Triboelectric Nanogenerator for Harvesting Environmental Energy," *ACS Nano* 15, no. 4 (2021): 6949–6960.
- [20] X. Liang, S. Liu, S. Lin, H. Yang, T. Jiang, and Z. L. Wang, "Liquid–Solid Triboelectric Nanogenerator Arrays Based on Dynamic Electric-Double-Layer for Harvesting Water Wave Energy," *Advanced Energy Materials* 13, no. 24 (2023): 2300571.
- [21] L. Xu, T. Z. Bu, X. D. Yang, C. Zhang, and Z. L. Wang, "Ultrahigh Charge Density Realized by Charge Pumping at Ambient Conditions for Triboelectric Nanogenerators," *Nano Energy* 49 (2018): 625–633.
- [22] T. Jiang, Y. Yao, L. Xu, L. Zhang, T. Xiao, and Z. L. Wang, "Spring-Assisted Triboelectric Nanogenerator for Efficiently Harvesting Water Wave Energy," *Nano Energy* 31 (2017): 560–567.
- [23] T. Jiang, H. Pang, J. An, et al., "Robust Swing-Structured Triboelectric Nanogenerator for Efficient Blue Energy Harvesting," *Advanced Energy Materials* 10, no. 23 (2020): 2000064.
- [24] X. Liang, T. Jiang, G. Liu, Y. Feng, C. Zhang, and Z. L. Wang, "Spherical Triboelectric Nanogenerator Integrated With Power Management Module for Harvesting Multidirectional Water Wave Energy," *Energy & Environmental Science* 13, no. 1 (2020): 277–285.
- [25] S. Gong, K. Li, J. Sun, J. Chen, and H. Guo, "Interfacial Droplet-Based Triboelectric Nanogenerator With Optimized Architecture for Highly Efficient Vibrational Energy Conversion," *Joule* 9, no. 1 (2025): 101763.
- [26] R. D. Cruise, K. Hadler, S. O. Starr, and J. J. Cilliers, "The Effect of Particle Size and Relative Humidity on Triboelectric Charge Saturation," *Journal of Physics D: Applied Physics* 55, no. 18 (2022): 185306.
- [27] S.-H. Chung, K. Cha, M. Song, et al., "Sub-Watt Power Triboelectric Generator via Polarization Switching Charge Carrier," *Nano Energy* 103 (2022): 107754.
- [28] W. D. Greason, Z. Kucerosky, S. Bulach, and M. W. Flatley, "Investigation of the Optical and Electrical Characteristics of a Spark Gap," *IEEE Transactions on Industry Applications* 33, no. 6 (1997): 1519–1526.
- [29] Z. Zhao, L. Zhou, S. Li, et al., "Selection Rules of Triboelectric Materials for Direct-Current Triboelectric Nanogenerator," *Nature Communications* 12, no. 1 (2021): 4686.
- [30] G. Min, Y. Xu, P. Cochran, N. Gadegaard, D. M. Mulvihill, and R. Dahiya, "Origin of the Contact Force-Dependent Response of Triboelectric Nanogenerators," *Nano Energy* 83 (2021): 105829.
- [31] T. Ji and A. Pachi, "Frequency and Velocity of People Walking," *Structural Engineer* 84, no. 3 (2005): 36–40.
- [32] T. Abdel-Baset, M. Elzayat, and S. Mahrous, "Characterization and Optical and Dielectric Properties of Polyvinyl Chloride/Silica Nanocomposites Films," *International Journal of Polymer Science* 2016, no. 1 (2016): 1707018, 13.